First principles study of the electronic and magnetic structures of U2Ni2SnH2

Samir F. Matar, Adel F. Al Alam

New Journal of Physics
The open-access journal for physics

First principles study of the electronic and magnetic structures of $U_2Ni_2SnH_2$

S F Matar[1] **and A F Al Alam**

CNRS, ICMCB, Université de Bordeaux, 87 avenue du Docteur Albert Schweitzer, 33608 Pessac Cedex, France
E-mail: matar@u-bordeaux1.fr

New Journal of Physics **10** (2008) 083013 (11pp)
Received 23 April 2008
Published 14 August 2008
Online at http://www.njp.org/
doi:10.1088/1367-2630/10/8/083013

Abstract. The electronic and magnetic properties and the chemical bonding in recently evidenced $U_2Ni_2SnH_2$ are self-consistently calculated within the local spin density-functional (LSDF) theory using the scalar-relativistic augmented spherical wave (ASW) method. Trends of the magnetism are discussed in terms of the changes brought by hydrogen within the pure U_2Ni_2Sn alloy system from both the volume expansion simulating negative pressure and the bonding between H and lattice constituents U, Ni and Sn pointing to a larger Ni–H bonding versus U–H. The ground state is found to be antiferromagnetic in agreement with experiment. Considering the relativistic effects of spin–orbit coupling an ordered magnetic moment, $m_U = 1\ \mu_B$ is calculated for U(5f), close to the experimental magnitude of $m_U = 0.83\ \mu_B$.

[1] Author to whom any correspondence should be addressed.

Contents

1. Introduction

The families of ternary 2 : 2 : 1 intermetallic systems U_2T_2X (T = 3d, 4d transition metal; X = Sn, In p-metal) are well known for exhibiting a wide variety of electronic and magnetic properties [1]–[3]. In these compounds, the formation of magnetic moments is governed by the degree of hybridization of the electronic valence states of uranium and those of the respective T and X ligands. The physical reasons for the varying hybridization strength can be seen in the bond lengths and in the crystal structure characteristics of these compounds. In uranium-based intermetallic systems, the mechanism of intra-band spin polarization of the 5f states depends on the so-called Hill critical distance, i.e. $d_{U-U} = 3.5$ Å [4]. Generally there is no intra-band spin polarization below this value as the 5f(U) band broadens due to the direct overlap of the 5f wave functions. Recent experimental work [5, 6] has shown that the 2 : 2 : 1 Sn-based intermetallic systems can absorb hydrogen with different amounts depending on the nature of T. The highest hydrogen uptake occurs for U_2Ni_2Sn with ∼2 H per formula unit (fu). In this case, we note that the hydrogen storage capacity for the material does not exceed 0.3 wt.% while that of the archetype hydride for applications, MgH_2, is 7.6 wt.%. Consequently, such intermetallic systems cannot be envisaged for energy storage for mobile applications, but could be relevant in stationary ones. However, issues in materials science fundamentals can justify their study.

With respect to the intermetallic U_2Ni_2Sn system, the expansion of the lattice due to hydrogen absorption should lead to a larger separation of 5f(U) states due to the reduction of the 5f–5f overlap. For instance, spin-fluctuation U_2Co_2X, shows different changes pertaining to an onset of long distance magnetic order upon hydrogenation [6]. However, the chemical interaction between the valence states of U, T and Sn on one hand and H on the other hand may induce a decrease of the magnetic polarization and, eventually, a loss of magnetization. The interplay of such effects can be addressed using computational tools based on the density functional theory (DFT) [7]–[9] as has been carried out in recent years for uranium-based intermetallic systems [10, 11]. Such effects are addressed here within the newly found $U_2Ni_2SnH_2$ system.

2. Theoretical framework of calculations

2.1. Computational methodology

An all-electron computational method was used in the framework of DFT [7]–[9]. These calculations are based on the local density approximation (LDA), as parametrized according to Vosko, Wilk and Nusair [12]. They were performed using the scalar-relativistic implementation of the augmented spherical wave (ASW) method (see [13, 14] and references therein). In the ASW method, the wave function is expanded in atom-centered ASWs, which are Hankel functions and numerical solutions of Schrödinger's equation, respectively, outside and inside the so-called augmentation spheres. In the minimal ASW basis set, we chose the outermost shells to represent the valence states and the matrix elements were constructed using partial waves up to $l_{\max}+1=4$ for U, i.e. U(5f) were considered within the basis set, $l_{\max}+1=3$ for Ni (Sn) and $l_{\max}+1=2$ for H. The completeness of the valence basis set was checked for charge convergence, i.e. less than 0.1 electron for $l_{\max}+1$. Self-consistency was achieved by a highly efficient algorithm for convergence acceleration [15]. The Brillouin zone integrations were performed using the linear tetrahedron method with up to 4096 **k**-points within the irreducible wedge [14, 16]. The efficiency of this method in treating magnetism and chemical bonding properties in transition-metal, lanthanide and actinide compounds has been well demonstrated in recent years [17]–[20].

2.2. Assessment of chemical bonding properties

To extract more information about the nature of the interactions between the atomic constituents from electronic structure calculations, different schemes are available, such as the crystal orbital overlap population (COOP) [21], the crystal orbital Hamiltonian population (COHP) [22] or the covalent bond energy (ECOV) [23] criteria. In this work, we use the COOP criterion based on the overlap population (OP): $c^*_{ni}(k)S_{ij}c_{nj}(k)=c^*_{ni}(k)\langle\chi_{ki}(r)|\chi_{kj}(r)\rangle c_{nj}(k)$, where S_{ij} is an element of the overlap matrix of the valence basis functions and $c_{nj}(k)$ are the expansion coefficients for the nth band. The partial COOP coefficients $C_{ij}(E)$ over two centers i and j are then obtained by integration of the above expression over the Brillouin zone

$$C_{ij}(E)=C_{ji}(E)=\frac{1}{\Omega_{\mathrm{BZ}}}\sum_n\int_{\mathrm{BZ}}\mathrm{d}^3k\,\mathrm{Real}\{c^*_{ni}(k)S_{ij}c_{nj}(k)\}\delta(E-\epsilon_{nk}),$$

where Ω_{BZ} is the Brillouin zone volume and Dirac δ serves as a counter of states. $C_{ij}(E)$ can be grossly designated as a density of states (DOS) function modulated by the OP. The chemical interaction is then labeled as bonding, antibonding or nonbonding according to the sign of the quantity between { } brackets, i.e. respectively, positive, negative and zero.

3. Calculational results and discussion

$U_2Ni_2SnH_2$ crystallizes in a tetragonal structure (space group P4/mbm) with 4 fu, similar to initial U_2Ni_2Sn, with $a=7.445$ Å and $c/a=0.506$. Within the structure sketched in figure 1, U, Ni and Sn are located respectively, at 4h, 4g and 2a Wyckoff positions [5]. Hydrogen atoms are distributed at four out of eight sites of 8k positions within U_3Ni tetrahedra which are coupled

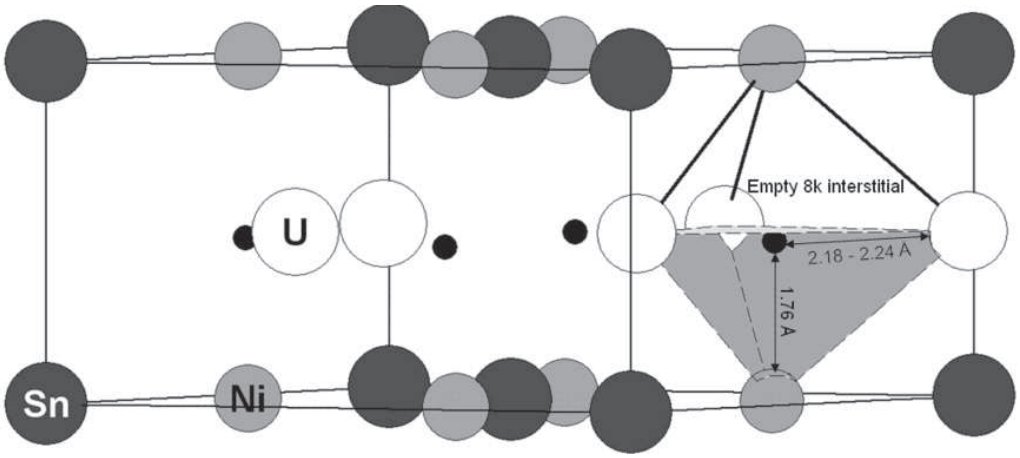

Figure 1. Sketch of the crystal structure of $U_2Ni_2SnH_2$ showing the face sharing U_3Ni tetrahedra; the one occupied by H is colored in gray. H atoms are drawn as small black spheres.

by sharing a face. Within each couple of these tetrahedra, the interatomic distance between two H atoms occupying the voids amounts to 0.2544 Å which is a too small separation with respect to the Switendick criterion ($d_{H-H} \geqslant 2.1$ Å) [24]. This explains the half-filling of the 8k sites. Further, it can be expected that hydrogen will mainly interact with Ni and U rather than with Sn.

The crystal parameters of $U_2Ni_2SnH_2$ given above were used as only input for the *ab initio* self-consistent calculations. In a first step, the calculations were carried out assuming a non-magnetic (NM) configuration (non spin-polarized, NSP), meaning that spin degeneracy was enforced for all species. However, such a configuration does not describe a paramagnet, which could be simulated for instance by a supercell entering random spin orientations over the different magnetic sites. Subsequent spin-polarized SP calculations (spin-only) lead to an implicit long-range ferromagnetic ordering. In order to provide a thorough description of the magnetic system, an antiferromagnetic (AF) configuration was also considered. The ground state configuration can be validated from the relative energies of the band theoretical calculations for both ferro- and antiferromagnetic configurations. Lastly, another set of computations was performed for a hydrogen-free model at the same volume of the experimental H-based system. This procedure evaluates the manner in which the volume expansion affects the magnetic behavior of uranium as well as the long range magnetic order.

3.1. Spin degenerate calculations

At self-consistent convergence little charge transfer was observed between the atomic species. For instance, in $U_2Ni_2SnH_2$ a departure of $\sim$0.2 electron occurs from U spheres to other constituents spheres. This slight transfer, not indicative of ionic effects—rarely observed in the framework of such calculations—signals a redistribution of the two s electrons of uranium over its three valence basis sets thus providing it with p and d character arising from its mixing with 3d(Ni) and 5p(Sn). This was already observed within the alloy system itself [20]. A further redistribution occurs upon hydrogen absorption with a larger s character within the valence band

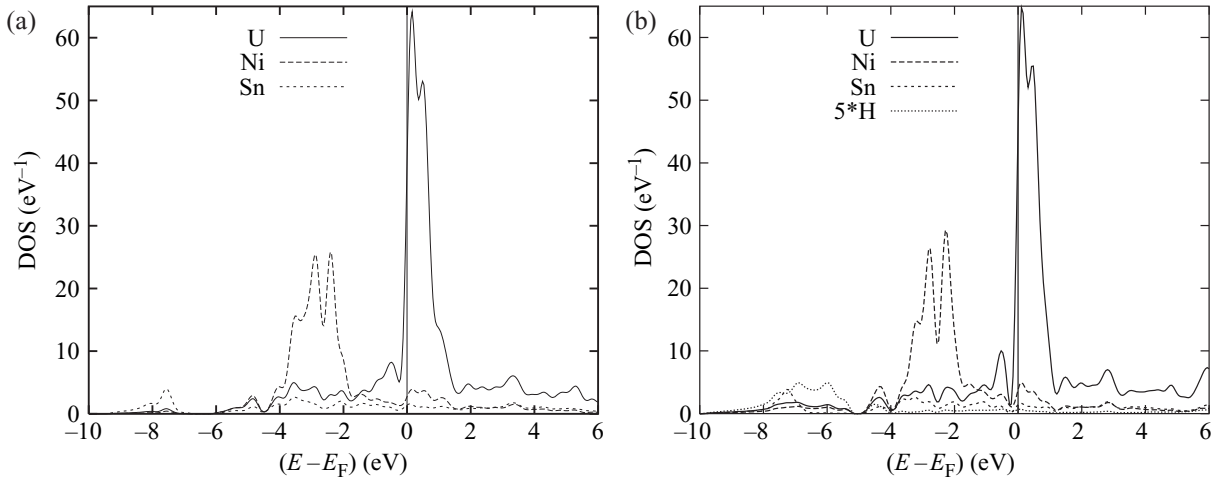

Figure 2. NM site projected DOS of U_2Ni_2Sn (a) and $U_2Ni_2SnH_2$ (b). In (b) H PDOS were artificially magnified five times for the sake of clarity.

(VB) as discussed within the DOS section below. Therefore one can argue that the major effect is that of the hybridization of the different valence states, not the charge transfer.

3.1.1. Site-projected DOS. The site-projected DOS (PDOS) for the H-based system are given in figure 2(b). In this plot and other ones in this paper, the Fermi level (E_F) is taken as zero energy. For the sake of comparison, the PDOS of U_2Ni_2Sn from previous calculations [20] are reproduced in figure 2. This will enable an insight into H influence to be obtained. From figure 2(b), showing the $U_2Ni_2SnH_2$ PDOS, the overall feature is that of a larger localization of U and Ni metal states. The hybridization between the different atomic constituents is observed within the itinerant part of VB ranging from -4 eV up to E_F. The uranium PDOS are seen to prevail through the large peak around E_F mainly due to the 5f states. The lower energy lying PDOS regions of the latter are crossed by E_F. Since the major part of these bands is unoccupied, they are found to be centered above E_F. This agrees with the low filling of the uranium f subshell by three electrons. Furthermore, this peak is more intense for $U_2Ni_2SnH_2$, with respect to the pure intermetallic system. This feature is connected with the larger PDOS value at E_F for the H-based system. Considering the charge distribution in U d states, it is found to be slightly unbalanced for intermetallic U_2Ni_2Sn with respect to the H-based system, i.e. $5f^{2.65}$ and $5f^{2.73}$. An electron population close to 3 for 5d(U) within the H-based system points to an atomic-like character of uranium. On the other hand, the PDOS of Ni is dominated by its 3d states centered around -3 eV. This is indicative of a larger localization with respect to U_2Ni_2Sn. Moreover, the 3d(Ni) states are closer to the Fermi level in the H-based system with respect to the Sn-based compound. This feature is brought by H, which provides additional electrons to the system, resulting in a larger width of the VB with respect to U_2Ni_2Sn. 5p(Sn) states are found in the energy range from -5 eV up to E_F characterized by their weak PDOS intensities with respect to U and Ni. They hybridize with 3d(Ni) states within the lower part of this region. Low energy lying 5s(Sn) states are observed around -8 eV within an energy range comprising itinerant U and Ni states as well as hydrogen broad states. The presence of hydrogen increases the itinerant part within the VB, especially for 7s(U) occupation which increases upon

hydrogenation. However, the major part of the bonding will be seen to occur in the energy range -6 eV, E_F as detailed below.

3.1.2. Analysis of the DOS within Stoner theory. In as far as 5f(U) states were treated as band states by our calculations, the Stoner theory of band ferromagnetism [9] can be applied to address the spin polarization. The total energy of the spin system results from the exchange and kinetic energies counted from a NM state. Formulating the problem at zero temperature, one can express the total energy as

$$E = \frac{1}{2}\left[\frac{m^2}{n(E_F)}\right][1 - \mathrm{I}n(E_F)].$$

Here I is the Stoner exchange integral, which is an atomic quantity that can be derived from spin-polarized calculations [25]; $n(E_F)$ is the PDOS value for a given species at the Fermi level in the NM state. The product $\mathrm{I}n(E_F)$ from the expression above provides a criterion for the stability of the spin system. The change from a NM configuration towards spin polarization is favorable when $\mathrm{I}n(E_F) \geqslant 1$. The system then stabilizes through a gain of energy due to exchange. From [26], the Stoner exchange integral value is given as I(U-5f) ~ 0.033 Ryd. Our computed $n(E_F)$ value of U(5f) for $U_2Ni_2SnH_2$ is 147 Ryd^{-1}, resulting in an $\mathrm{I}n(E_F)$ value of 4.8. Such a large magnitude of the Stoner product for the f states indicates their major contribution to the magnetic instability for the H-based system. This will be checked within the spin-polarized calculations whereby a finite magnetic moment is expected to be carried by 5f(U) states. On the other hand, the H-free alloy model has a $n(E_F)$ value of 129 Ryd^{-1} for U(5f). This results in a Stoner product value of 4.3, which establishes a clear tendency towards magnetic moment onset. Nevertheless, the magnitude of its Stoner product is lower with respect to its H-based model analogue, which emphasizes the contribution of H interactions with the other atomic species to the arising of the magnetic ordering over the volume expansion.

3.1.3. Bonding characteristics. Chemical bonding properties can be addressed on the basis of the spin-degenerate calculations. This is due to the fact that the spin-polarized electronic bands, to a large extent, result from the spin-degenerate bands by a rigid energy splitting. Figure 3(a) shows the COOP plots for metal–metal interactions within $U_2Ni_2SnH_2$. A visual inspection of figure 3(a) shows that the dominant interaction within the VB results from the U–Ni interaction which is bonding. The second most bonding interaction is U–Sn, then for Ni–Sn, a bonding character is observed from -4 to -2 eV, followed by an antibonding behavior, from -2 eV up to E_F, which cancels the bonding behavior. This is related to the fact that Ni valence states are mainly full and extra electrons will be within unfavorable antibonding states. Thus the dominant feature within VB is the bonding one, and the H-based system is stable. To further explain this behavior, the interatomic distances are addressed, whereby a binding character is proportional to the inverse of the separation between the atomic constituents. For instance, the separation between U and Ni, as estimated by the calculations performed for $U_2Ni_2SnH_2$, ranges from 2.79 to 2.97 Å while Sn–Ni and Sn–U have interatomic distances values such as 2.94 and 3.32 Å, respectively. From this one can establish the relationship with the bonding properties mentioned earlier. In as far as the computed value of 2.97 Å for some U–Ni distances is larger with respect to the Sn–Ni separation of 2.94 Å, the order of the bonding strengths for the respective interactions should be affected, which is not the case. This can be explained by the amount of Sn atoms present within the system given by the occupancy ratio of 2 : 2 : 1 for

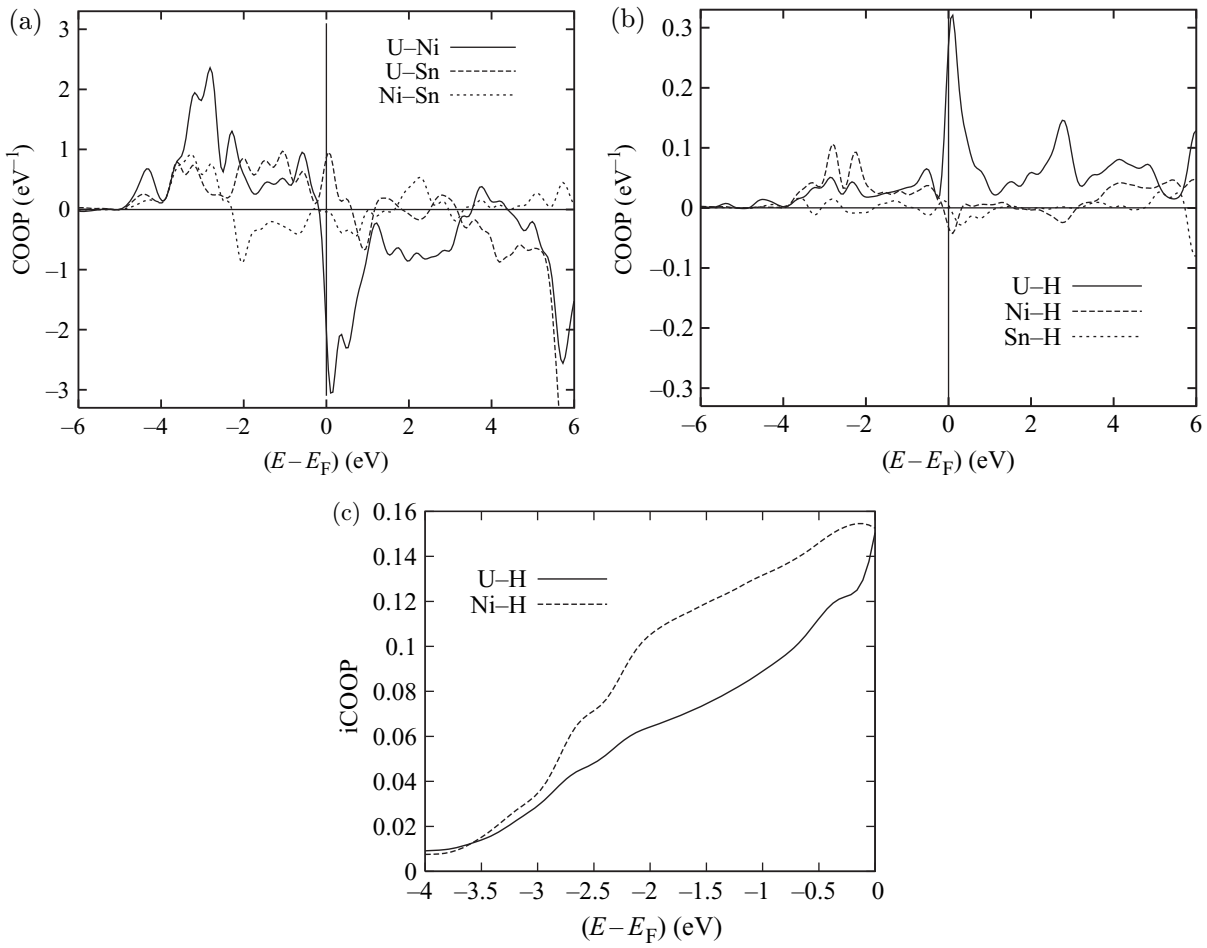

Figure 3. Chemical bonding within $U_2Ni_2SnH_2$: NM COOP for metal–metal interactions (a) and metal–H interactions (b). Intregrated COOP for metal–H interactions are also included (c). U(5f) states are included for all panels.

U, Ni and Sn, respectively. Moreover, Ni binds with hydrogen due to the positioning of the former within the interstitial surrounding of the latter. This is shown in figure 3(b) detailing the metal–hydrogen interactions where Ni–H ones are the most binding followed by U–H ones within VB. This is further confirmed by the ratio of the integrated COOP surfaces for both interactions (see figure 3(c)), within the energy range lying from −4 eV to E_F in VB, where Ni–H area is calculated to be ∼1.4 times larger than its U–H analogue. Again, the interatomic distances confirm these binding tendencies where the Ni–H separation is clearly the shortest, with a value 1.76 Å followed by U–H separations ranging from 2.18 to 2.24 Å. Finally, it is important to mention that metal–H interactions which are ∼10 times less intense than the metal–metal ones (figure 3(a)) are mainly of bonding character throughout the VB. This points to the stabilizing role brought by the hydrogen atoms inserted within U_2Ni_2Sn. This feature is further confirmed with the magnitude of the formation energy (ΔE) for the H-based system given as

$$\Delta E = \tfrac{1}{2}[E(U_2Ni_2SnH_2) - E(U_2Ni_2Sn)] - \tfrac{1}{2}E(H_2),$$

Table 1. Calculated results for U_2Ni_2Sn and $U_2Ni_2SnH_2$: ΔE values are for total energy differences with respect to NSP values of −260 557.260 371, −260 561.586 68 and −260 557.292 800 Ryd for the pure intermetallic, H-based and H-free systems, respectively. Magnetic moments of U, Ni and Sn are also presented for the different configurations.

	U_2Ni_2Sn	$U_2Ni_2SnH_2$	H-free $U_2Ni_2SnH_2$
ΔE_{NSP} (Ryd)	0	0	0
ΔE_{SP} (10^{-4} Ryd)	−221	−259	−300
ΔE_{AF} (10^{-4} Ryd)	−254	−281	−346
m_U^{SP} (μ_B)	1.497	1.405	1.784
m_U^{AF} (μ_B)	±1.670	±1.678	±1.831
m_{Ni}^{SP} (μ_B)	−0.055	−0.072	−0.081
m_{Ni}^{AF} (μ_B)	0	±0.019	0
m_{Sn}^{SP} (μ_B)	−0.010	−0.015	0.006
m_{Sn}^{AF} (μ_B)	0	±0.001	0

where $E(U_2Ni_2SnH_2)$ represents the total energy of the H-based system (−260 561.586 681 Ryd), $E(U_2Ni_2Sn)$ the energy of the intermetallic system (−260 557.260 371 Ryd) and $E(H_2)$ the energy of the dihydrogen molecule (−0.485 Ryd), the latter being computed by considering a cubic supercell of lattice parameter 4.5 Å. This amounts to a formation energy of −0.839 Ryd fu^{-1}, in favor of a bonded hydrogen within the lattice. Compared with the literature, ΔE magnitude is ∼2.4 times smaller with respect to the 1 : 1 : 1 $ThNiInH_{1.333}$ formation energy [27].

3.2. Spin-polarized configurations and long-range magnetic orders

3.2.1. Ferromagnetic configuration. From the NSP calculations and their analysis within the Stoner mean-field theory of band ferromagnetism, it has been established that the H-based system is stable in such a configuration for H content close to the experiment [5], i.e. $U_2Ni_2SnH_{1.8}$. Consequently, spin-polarized calculations were carried out, assuming implicitly a hypothetic ferromagnetic order. This is done by initially allowing for two different spin occupations, then the charges and the magnetic moments are self-consistently converged. The relative energy difference (ΔE_{SP}) of the spin-polarized calculations for $U_2Ni_2SnH_2$, with respect to its NM energy, given in table 1, favors the ferromagnetic state. Theoretical NM computations of the H-based system reported a magnetic instability. Spin-polarized calculations confirmed these tendencies by identifying a finite spin only magnetic moment of 1.40 μ_B carried by 5f(U) states. These results are illustrated in figure 4(a) showing the site and spin projected DOS of $U_2Ni_2SnH_2$. The exchange splitting is observed for uranium. Its magnitude extracted from the energy difference between the Hankel spherical functions which designate the middle of the band in ASW formalism, for $l = 3$(U5f), amounts to 0.049 Ryd.

3.2.2. AF configuration. The experimental findings suggested an AF ground state configuration for $U_2Ni_2SnH_2$. In order to check for the nature of the magnetic ground state, AF calculations were carried out by using a supercell built from two simple cells along the *c*-axis. These

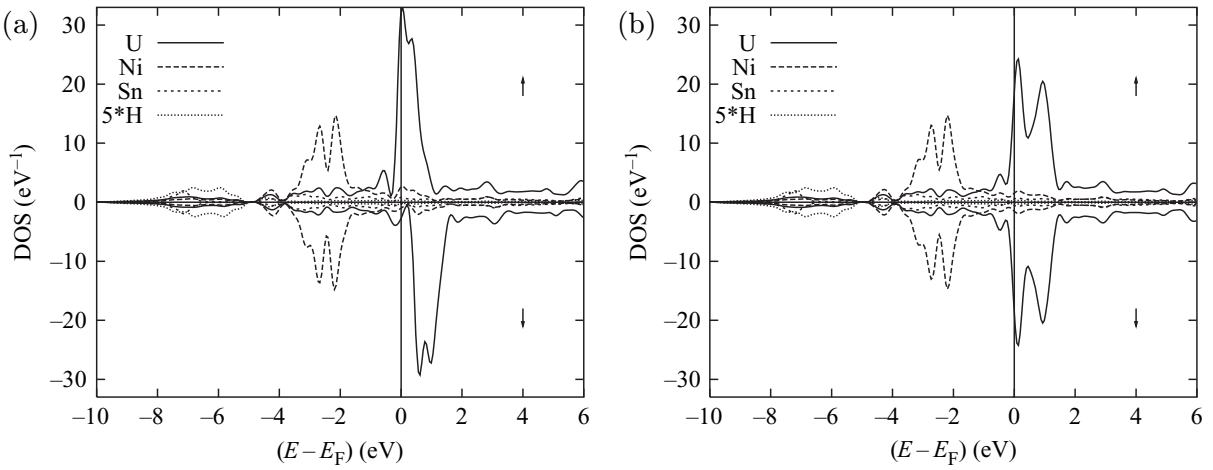

Figure 4. Spin-polarized site projected DOS of $U_2Ni_2SnH_2$ for both ferro- (a) and AF configurations (b).

two structures were used to distinguish between the up- and down-spin atoms. The site- and spin-projected DOS of AF $U_2Ni_2SnH_2$ are sketched in figure 4(b). An overall similarity with the PDOS of the ferromagnetic H-based system (see figure 4(a)) is observed, when it comes to Ni, Sn and H PDOS shapes. But for U PDOS a less intense and narrower peak is observed at E_F. This is significant of a more important localization which can be explained from a detailed analysis of the electron populations. Also, there is full compensation between ↑ and ↓ spin populations, i.e. no energy shift between them, with a spin moment of U of $\pm 1.678\,\mu_B$, higher than in the SP configuration. This is concomitant with a value of 0.058 Ryd for the exchange splitting at U, higher than in the ferromagnetic configuration. Then, at self-consistency, the total energy difference ($\Delta E = E_{Ferro} - E_{AF}$) have a value of 2.2×10^{-3} Ryd, which favors the AF ordering, thus pointing to an AF ground state for $U_2Ni_2SnH_2$. Furthermore, the energy differences values for H-free $U_2Ni_2SnH_2$ (see table 1) show that the volume expansion is favorable with respect to an AF ground state.

3.2.3. Spin–orbit coupling effects. It is known that the relativistic effects like spin–orbit coupling (LS) have considerable influence on the formation and the magnitude of magnetic moments in narrow-band systems such as those based on 5f elements [20]. In fact, the size of the LS splitting is within the order of magnitude of the 5f bandwidth. Moreover, the atomic magnetic moment treated in such a framework consists of contributions from spin as well as orbital moments. While the former is obtained from our ferro- and antiferromagnetic calculations, i.e. 1.405 and $\pm 1.678\,\mu_B$ respectively, the latter is obtained from a former work on 2 : 2 : 1 uranium-based systems [20] using fully relativistic calculations, $m_L^U = -2.7\,\mu_B$. It should be mentioned that the orbital moment of U stems from an f occupation of about 2.74 (2.75) electrons, for ferromagnetic (AF) calculations, whose orbital moment ($-2.7\,\mu_B$) comes close to that of an atomic orbital, namely $3\,\mu_B$ as expected from Hund's second rule. This reflects the atomic-like character of the 5f(U) shell. The total moment can then be calculated from the sum of both spin and orbital moments which align oppositely due to Hund's 3rd rule for a less than half-filled f subshell. The resulting values are -1.3 and $\pm 1.02\,\mu_B$ for ferro- and antiferromagnetic configurations, respectively. The latter compares well with the experimental value of $0.83\,\mu_B$ [5]. Furthermore, applying these LS corrections to the U_2Ni_2Sn intermetallic

system, results in a magnetic moment carried by uranium amounting to 1.03 μ_B which is close to the experiment (1.05 μ_B) [5]. This moment has a slightly larger magnitude with respect to the H-based system, which reflects the lower Néel temperature for the AF ordering of the intermetallic system ($T_N = 26$ K) with respect to $U_2Ni_2SnH_2$ ($T_N = 87$ K).

4. Conclusion

In this work, we have undertaken theoretical investigations of the hydrogen intake effects within the 2 : 2 : 1 Sn-based U_2Ni_2Sn system. The electronic and magnetic structures calculated with all-electron computations within the DFT led to the DOS and chemical bonding properties for $U_2Ni_2SnH_2$ being addressed. A reduction in both 5f–5f overlap and 5f bandwidth led to prediction of an enhanced magnetic moment on uranium 5f states. However, an analysis of the chemical interactions of U and Ni with H led to a reduced moment with respect to a hydrogen-free model system. Hydrogen is also found to be favorably bound within $U_2Ni_2SnH_2$. From the energy differences, the ground state is found to be AF. The calculated magnetization magnitude $\sim 1\ \mu_B$ is obtained in agreement with experiment (0.83 μ_B) when the relativistic effects of spin–orbit coupling are accounted for.

Acknowledgments

Computational facilities were provided within the intensive numerical simulation facilities network M3PEC of the University Bordeaux 1 partly financed by the 'Conseil Régional d'Aquitaine'. Exchange and discussions with K Miliyanchuk are acknowledged.

References

[1] Purwanto A *et al* 1994 *Phys. Rev.* B **50** 6792
[2] Mirambet F, Gravereau P, Chevalier B, Trut L and Etourneau J 1993 *J. Alloys Compouds* **199** L1
[3] Mirambet F, Chevalier B, Fournés L, Gravereau P and Etourneau J 1993 *J. Alloys Compounds* **203** 29
[4] Hill H 1970 *Plutonium 1970 and Other Actinides* ed W N Miner (New York: Mat. Soc. Aime) p 2
[5] Miliyanchuk K, Havela L, Pereira L C J, Gonçalves A P and Prokeš K 2007 *J. Magn. Magn. Mater.* **310** 945
[6] Miliyanchuk K, Havela L, Kolomiets A V and Andreev A V 2005 *Physica* B **359** 1042
[7] Hohenberg P and Kohn W 1964 *Phys. Rev.* B **136** 864
[8] Kohn W and Sham L J 1965 *Phys. Rev.* A **140** 1133
[9] Kübler J and Eyert V 1992 *Materials Science and Technology* vol 3A *Electronic and Magnetic Properties of Metals and Ceramics Electronic Structure Calculations* Part I ed K H J Buschow (Weinheim: VCH) pp 1–145
[10] Matar S F and Siruguri V 2007 *J. Alloys Compounds* **436** 34
[11] Matar S F, Siruguri V and Eyert V 2006 *J. Magn. Magn. Mater.* **305** 264
[12] Vosko S H, Wilk L and Nusair M 1980 *Can. J. Phys.* **58** 1200
[13] Williams A R, Kübler J and Gelatt C D 1979 *Phys. Rev.* B **19** 6094
[14] Eyert V 2007 *The Augmented Spherical Wave Method—A Comprehensive Treatment, Lecture Notes in Physics* vol 719 (Berlin: Springer)
[15] Eyert V 1996 *J. Comput. Phys.* **124** 271
[16] Blöchl P E 1994 *Phys. Rev.* B **50** 17953
[17] Chevalier B and Matar S F 2004 *Phys. Rev.* B **70** 174408
[18] Eyert V, Laschinger C, Kopp T and Frésard R 2004 *Chem. Phys. Lett.* **385** 249

[19] Matar S F, Gaudin E, Chevalier B and Pöttgen R 2007 *Solid State Sci.* **9** 274
[20] Matar S F and Mavromaras A 2000 *J. Solid State Chem.* **149** 449
[21] Hoffmann R 1987 *Angew. Chem. Int. Ed. Engl.* **26** 846
[22] Dronskowski R and Blöchl P E 1993 *J. Phys. Chem.* **97** 8617
[23] Bester G and Fähnle M 2001 *J. Phys: Condens. Matter* **13** 11541
[24] Switendick A E 1979 *Z. Phys. Chem.* **117** 89
[25] Janak J F 1977 *Phys. Rev.* B **16** 255
[26] Matar S F and Eyert V 1997 *J. Magn. Magn. Mater.* **166** 321
[27] Vajeeston P, Ravindran P, Vidya R, Kjekshus A and Fjellvåg H 2005 *Europhys. Lett.* **72** 569